# Computer simulation and experimental investigation of sheet metal bending using laser beam scanning

Z. Hu, M. Labudovic, H. Wang, R. Kovacevic *

*Department of Mechanical Engineering, Southern Methodist University, P.O. Box 750337, Dallas, TX 75275-0335, USA*

## Abstract

Computer simulation and experimental investigation of the sheet metal bending into a V-shape by the laser beam scanning without an external force exerted onto it have been performed. A 3-D FEM simulation has been carried out, which includes a non-linear transient indirect coupled thermal-structural analysis accounting for the temperature dependency of the thermal and mechanical properties of the materials. The bending angle, distribution of stress–strain, temperature and residual stresses have been obtained from the simulations. The sheet metal bending had been performed for different materials, thicknesses, scanning speeds and laser powers. The measurement of real-time temperature and bending angle was carried out. The bending angle is affected by the mechanical and thermal properties of the sheet metal material, the process parameters, and the output of laser energy. The bending angle is increased with the number of laser beam scanning passes and is the function of the laser power and the laser beam scanning speed. The simulation results are in agreement with the experimental results. © 2001 Elsevier Science Ltd. All rights reserved.

*Keywords:* Laser forming; Simulation; Bending; Finite element method

## 1. Introduction

Laser metal-forming is a promising technology in manufacturing, such as in the automobile, shipbuilding, and aerospace industries. The rapid, flexible and low-cost metal-forming can improve the competitiveness of these industries [1–7]. Laser forming technology began in the 1980s, and in that time, the development of laser-forming technology was more concentrated on

* Corresponding author. Tel.: +1-214-768-4865; fax: +1-214-768-0812.
   *E-mail address:* kovacevi@seas.smu.edu   (R. Kovacevic).

experimental studies [8–12]. In the 1990s, more work has concentrated on analytical simulation [13–25]. It was concluded that the main and most difficult problem faced is not just to form the metal to a desired accuracy, but to achieve it in an acceptably short time, in order to satisfy economic requirements. One way to achieve this is to speed up the process of metal-forming by hardware; this involves development of a high-power laser in order to form the metal. Another way is to develop predictive numerical models to improve the design method of the process, from the viewpoint of software, so as to improve the control programs.

The major problem of developing the laser-forming technology is that the process parameters must be determined before using the laser to form sheet metal into the prescribed shapes. Unfortunately, the relationship between the heating pattern and process parameters from one side and the bending angle from the other side is not well established. So the laser metal-forming process has been developed by using trial and error or empirical methods. This, however, proves to be expensive and time consuming. In the current competitive environment, the cost of the product is critical for survival in the industry. The key to improving the manufacturing processes, and hence to meeting the demand of lower cost and higher quality and productivity in commercial competitions, is to acquire detailed knowledge in the given process. Fortunately, the numerical techniques such as the finite element method (FEM) are revolutionizing the conventional trial-and-error methods in industry today. These methods have proved to be very useful in product development and process design, and have improved the quality of the products and our capability of explaining phenomena leading to defects in the processes.

In this article, the new design method of the laser sheet metal bending process based on computer simulation and experimental investigation is described.

## 2. Governing equations

In order to analyze the movement and deformation of the configuration in the finite element method, supposing the equilibrium states at all the time steps concerned from time 0 to $t$ have been obtained, the equilibrium equation at time $t+\Delta t$ can be expressed as follows, according to the virtual work principle [26]:

$$\int_v \sigma \cdot \delta\varepsilon \cdot \mathrm{dV} = \int_v q \cdot \delta u \cdot \mathrm{dV} + \int_s p \cdot \delta u \cdot \mathrm{dS} \tag{1}$$

where $\sigma$ and $\varepsilon$ are stress and strain tensors in updated Lagrange configuration descriptions, respectively, $q$ and $p$ body force and surface pressure, respectively, and $\delta u$ the virtual displacement. Discretization of this problem is accomplished by means of the standard finite element procedure. After aggregation, we have a group of nonlinear equations that require the Newton–Raphson method to linearize them:

$$[K]\{\Delta u\} = \{F^a\} - \{F^{nr}\} \tag{2}$$

where $[K] = \int_v [B]^{\mathrm{T}}[D^{ep}][B]\mathrm{dV}$ is the tangential stiffness matrix, $[B]$ the general geometric matrix, $[D^{ep}]$ the elasto-plastic stress-strain matrix, $\{\Delta u\}$ the displacement incremental at the element nodes, $\{F^a\}$ the applied force vector, and $\{F^{nr}\} = \int_v [B]^{\mathrm{T}}\{\sigma\}\mathrm{dV}$ Newton–Raphson restored force vector.

For the thermo-mechanical coupled system, the thermal equilibrium equation for analysis of heat transfer can be written as

$$k\left(\frac{\partial^2 T}{\partial x^2}+\frac{\partial^2 T}{\partial y^2}+\frac{\partial^2 T}{\partial z^2}\right)+\dot{q}=\rho c\dot{T} \tag{3}$$

where $\rho$ and $c$ are density and specific heat of the material, respectively, $k$ the heat conductivity and $\dot{q}$ the rate of heat generation. Here, $\dot{q}$ is mainly considered as the heat source generated by laser beam scanning.

To get the solution from the thermal equilibrium equation, boundary conditions and initial conditions are needed. The basic FEM equations for the thermal problem can be derived from the thermal equilibrium equation

$$[C]\{\dot{T}\}+[K_T]\{T\}=\{Q\} \tag{4}$$

where $[C]=\int_V \rho c[N][N]^T dV$ is the heat capacity matrix, $[N]$ the shape function matrix, $[K_T]=\int_v k[B][B]^T dV$ the heat conduction matrix, $\{T\}$ and $\{\dot{T}\}$ nodal temperature vector and nodal temperature rate vector, respectively, and $\{Q\}$ the heat flux vector.

The basic equation for thermo-mechanical coupled calculation is as follows:

$$\begin{bmatrix}[0] & [0]\\ [0] & [C]\end{bmatrix}\begin{Bmatrix}\{\dot{u}\}\\ \{\dot{T}\}\end{Bmatrix}+\begin{bmatrix}[K] & [0]\\ [0] & [K_T]\end{bmatrix}\begin{Bmatrix}\{u\}\\ \{T\}\end{Bmatrix}=\begin{Bmatrix}\{F\}\\ \{Q\}\end{Bmatrix} \tag{5}$$

where $\{F\}$ is the force vector, including applied nodal force and the force caused by thermal strain.

## 3. Model of sheet bending by laser beam scanning

Being irradiated by a laser beam of high power density, which obeys a normal distribution, a workpiece absorbs a part of the laser energy on the surface. The laser beam diameter is shown as the diameter in which the power density is reduced from the peak value by a factor of the square of the natural exponent ($\mathbf{e}^{-2}$). The thermal energy is conducted into the material and temperature distribution and stress-strain distribution can be simulated. Fig. 1 shows the model of laser beam scanning on the sheet metal [11].

During the sheet metal bending process, the temperature distribution and the temperature gradient are dependent on many technological parameters and material properties such as the thermal flux density, the metal absorption on the surface, as well as the heating time. During the simulation, the thermal load is given in the form of the thermal flux density which obeys a normal distribution as follows [15]:

$$I=\frac{2AP}{\pi r_b^2}\exp\left(-\frac{2r^2}{r_b^2}\right) \tag{6}$$

where $I$ is the thermal flux density of the laser beam, $A$ is the absorptivity on the sheet metal surface, $P$ is the laser beam power, $r_b$ is the laser beam radius and $r$ is the distance from the center of the laser beam. So the mean thermal flux density within the area of the laser beam scanning on the sheet metal surface is
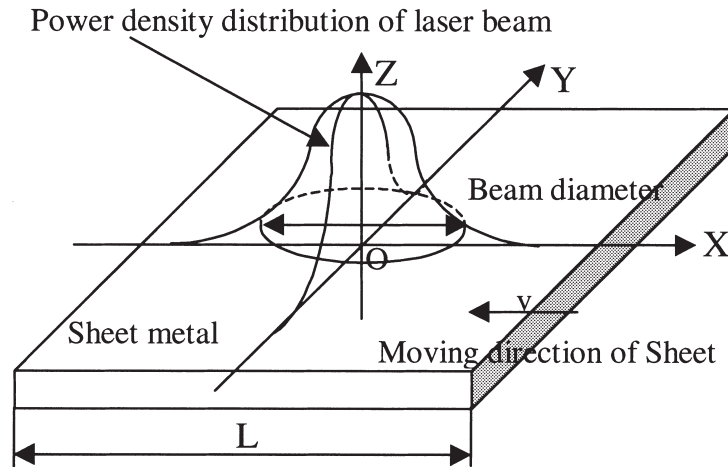
Power density distribution of laser beam

Fig. 1.   Model of laser beam scanning on the sheet metal.

$$I_m = \frac{1}{\pi r_b{}^2} \int\limits_0^{r_b} I(2\pi r)\mathrm{d}r = \frac{2\pi}{\pi r_b{}^2} \int\limits_0^{r_b} \frac{2AP}{\pi r_b{}^2} \exp\left(-\frac{2r^2}{r_b{}^2}\right) r\mathrm{d}r = \frac{0.865AP}{\pi r_b{}^2} \tag{7}$$

The heating time $t$ depends on the relative motion $v$ between workpiece, laser beam and the laser beam radius $r_b$ as follows:

$$t = 2r_b/v \tag{8}$$

The most important parameters on thermo-structural calculation were referred from [11,15,17,27,28].

## 4. Experimental procedure

The experimental set-up for sheet metal bending by laser beam scanning is shown in Fig. 2. The CW Nd-YAG laser is controlled by a computer control system. The defocused laser beam is 2 mm in diameter. The sheet metal sample is scanned forward and backward by moving the sample with respect to the stationary laser beam. The width of the samples are 50 mm, and the scanning width is 80 mm, 15 mm wider than the samples on each side. Different laser powers and scanning speeds are used. The bending angle was measured on-line with an integrated bending angle measuring system. The temperature variation was measured online by a thermo-couple measuring system. Two kinds of sheet materials, aluminum and AISI 304 stainless steel, were used. The experimental conditions are listed in Table 1.
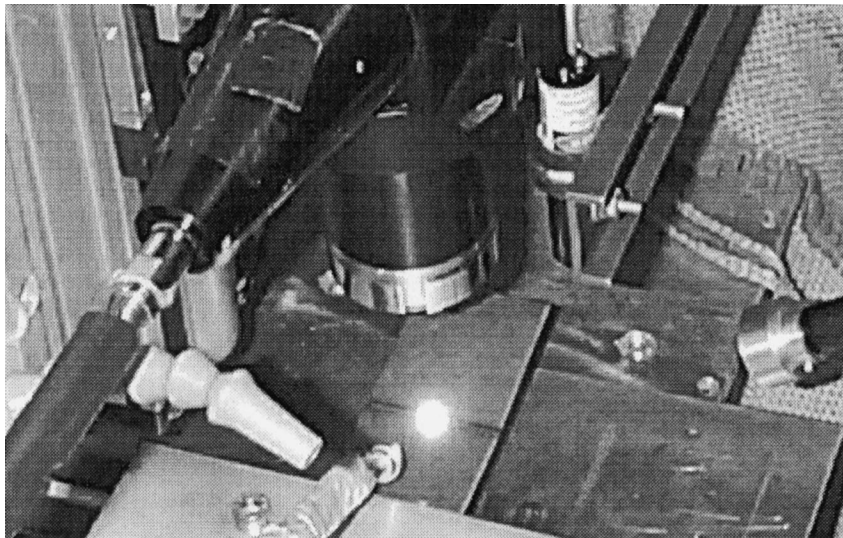
Fig. 2.  Experimental set-up for sheet bending by laser beam scanning.

Table 1
The experimental conditions

| Materials | Size (mm) | Laser power (W) | Scanning speed (mm/s) |
|---|---|---|---|
| Al | 50×100×1 | 800, 500, 250 | 10 |
| | 50×100×1 | 500 | 10, 20, 40 |
| | 50×100×1.5 | 500 | 10 |
| | 50×100×2 | 500 | 10 |
| AISI 304 | 50×100×0.75 | 250 | 20, 40, 60 |
| | 50×100×1.5 | 500, 250 | 10 |
| | 50×100×1.5 | 250 | 10, 20 |
| | 50×100×3 | 250 | 20 |

## 5. Measurement of bending angle

In the performed experiments, the bending angles were measured on-line with an integrated machine vision measuring system, as shown in Fig. 3. The measuring system is characterized by
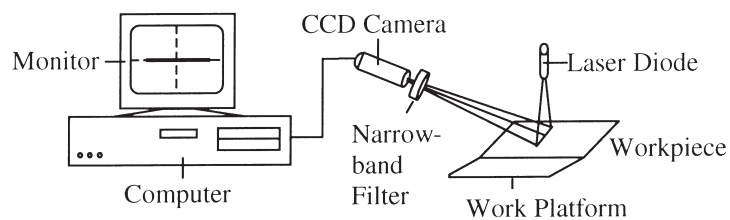


Fig. 3.  Schematic configuration of the bending angle measuring system.

the following features: it is non-contact, real-time, and highly accurate. The system consists of a CCD camera and a laser diode with a line generator. The image is acquired by using a 768 (horizontal) × 494 (vertical) array CCD camera with a focal length of 15 mm. The CCD image plane size is 6.54 mm (horizontal) × 4.89 mm (vertical). A narrow-band optical interference filter, with a central wavelength of 674 nm and FWHM of 5 nm, is used to block most of the ambient light. A frame grabber is used to delivered images to a PC with an acquisition rate of 30 frames per s. Each image is composed of 640 (horizontal) × 480 (vertical) 8-bit pixels.

Images in a CCD camera are formed by focusing the light coming from an object through the optical lens into an electronic device with arrays of light-sensitive elements. The behavior of the light as it passes through the lens can be described by the so-called "pinhole" lens model. If, for a given camera, the parameters of the pinhole model and the position in space of objects relative to the camera are known, then the exact location of the image on the CCD plane of every object point can be determined.

In the working platform and the image coordinate system, as shown in Fig. 4, because $O'Y'$ is parallel to $OY$, the triangle $O'PB'$ is similar to the triangle $OPB$, so the coordinates of $A'$ can be calculated as follows:

$$X_{A'} = OP\cos\theta(OO' - Z_A\sin\theta)/(OP - Z_A\sin\theta) \tag{9}$$

$$Z_{A'} = Z_A + (OP\sin\theta - Z_A)(OO' - Z_A\sin\theta)/(OP - Z_A\sin\theta) \tag{10}$$

Because $O'A'$ is the projection of $OA$ in the $O'$-$X'Y'Z'$ coordinate system, the distance from $O'$ to $A'$ is calculated

$$|O'A'| = \sqrt{(OO'\cos\theta - X_{A'})^2 + (OO'\sin\theta - Z_{A'})^2} \tag{11}$$

The relation between $Z'_{A'}$ and $Z_A$ is

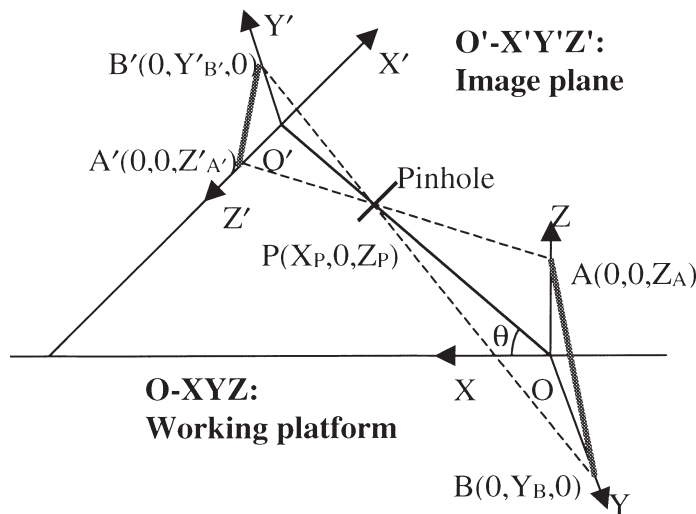$$Z'_{A'} = Z_A \cdot OP\cos\theta\sqrt{1 + \sin^2\theta}/(OP - Z_A\sin\theta) \tag{12}$$



Fig. 4.   Relationship between working platform and image coordinate system.

Because A and B are arbitrarily chosen, so

$$Y' = Y \cdot O'P / OP \tag{13}$$

$$Z' = Z \cdot O'P \cos\theta \sqrt{1 + \sin^2\theta} / (OP - Z\sin\theta) \tag{14}$$

## 6. Results and discussion

Computer simulation of the laser-forming [30] process is complex and difficult. The main steps of the analysis are the thermal analysis step and the structural analysis step. For the analyses, the finite element code ANSYS was used. In order to calculate the thermo-structural coupled field with large plastic deformation in ANSYS, an indirect coupled-field analysis, (i.e. two sequential analyses) was performed. The flow chart of the FEM simulation is shown in Fig. 5. In this method, the results from the transient thermal analysis for nodal temperatures were read and applied as loads for the structural analysis. Therefore, the calculation of temperature distribution is critical for the calculation of stress-strain distribution.

For this reason, temperatures at the bottom surface of the workpiece referring to the central point of the plate in the scanning line were measured in real-time to check and modify the parameters used in computer simulation models. The initial condition for simulation and experiment is that the whole specimen is at room temperature (25°C). The laser beam heating is applied as the surface heat source absorbed by the target, so the boundary conditions of the top surface
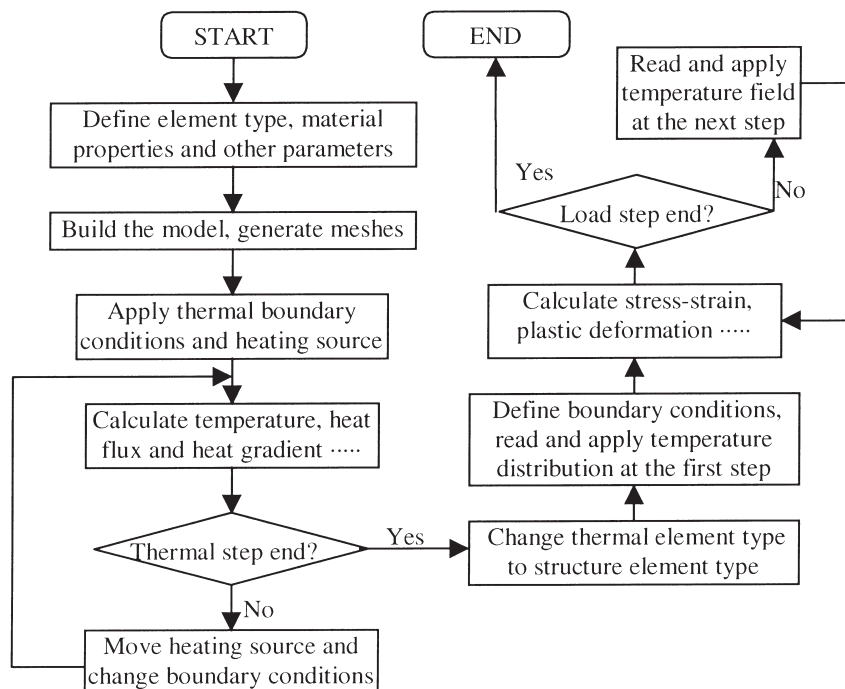


Fig. 5.   Flow chart of FEM simulation.

irradiated by the laser beam are considered as a moving surface thermal flux. The simulation results were compared with the experimental results as shown in Fig. 6 for AISI 304 and Fig. 7 for aluminum. The width of the samples are 50 mm, and the scanning width is 80 mm (15 mm wider than the samples in each side), and the scanning speed is 10 mm/s. In Fig. 6, due to experimental error, the measuring point is offset for 2.5 mm with respect to the heating line. A change in the thermal conductivity of the material yields a different temperature distribution pattern in the workpiece [29]. AISI 304 stainless steel, a poor conductor of heat, shows that the temperature rises rapidly when the measuring point is being heated and drops slowly when the heating source is moving away from it; aluminum, a good conductor of heat, shows that the temperature rises up relatively smoothly when the measuring point is being heated and drops relatively quickly when the heating source is moving away from it. The temperature difference along the sheet thickness of aluminum is smaller than that of AISI 304. The simulation results are also shown in the same figure.

Fig. 8 shows the temperature distribution during the first pass and the second pass in the three different profiles [i.e. in the top view surface (X-Y plane), in the front view cross section (X-Z plane), and in the left side view cross section (Y-Z plane)], by computer simulation. The points of maximum temperature and the maximum heating rate are in the rear and in the front of the center of the beam, respectively. The temperature gradient in the front of the center of the beam is steeper than that in the rear.

Fig. 9 shows the distribution of plastic strain $\varepsilon_y^p$ during the first scanning. It can be observed that at the point of the top surface in the central line, when it starts to be heated, a tensile plastic strain appears (from $t=2.3$ s to $t=2.4$ s). The compressive plastic deformation has initiated at $t=2.4$ s and continues to increase until $t=2.6$ s when the maximum temperature is achieved. This time point with maximum compressive plastic strain ($t=2.6$ s) corresponds to the maximum achieved temperature, while at the bottom surface, a relatively smaller tensile plastic strain appears and stays unchanged during the scanning. The distribution of this plastic strain is responsible for the achieved bending angle. It is obvious that the bending process begins firstly with a minus bending angle (i.e. bending opposite to the laser beam), and then immediately bends towards the laser beam. The width of the plastically deformed zone on the irradiated surface is about the diameter of the laser beam. The residual strain is negative at the top surface and is positive at the bottom surface, which explains the formation of the bending angle towards the laser beam.

Fig. 10 shows the distribution of stress $\sigma_y$ during the first scanning. The stress is tensile from the top surface to the bottom in the heated zone at the beginning of the heating period (from $t=0$ to $t=2.3$ s) and then changed rapidly; the stress at the points considered are dropped to a maximum compressive stress (from $t=2.3$ s to $t=2.6$ s). The maximum compressive stress ($t=2.6$ s) also corresponds to the maximum achieved temperature. The stress at the points of the bottom and middle surface is increased smoothly to a relatively smaller compressive stress (from $t=2.8$ s to $t=5.0$ s), and the stress on the top surface is increased rapidly to a maximum tensile stress. The obtained residual stresses cause tension at the top surface of the sheet metal and compression in the middle surface and the bottom surface of the sheet metal in order to keep force equilibrium.

The bending angle history is shown in Figs. 11–13. The simulated bending angles were compared with measured ones. The experimental results are in agreement with the simulated ones: the bending is in the direction away from the laser beam during heating and toward the laser beam during cooling under the given process parameters and the experimental conditions. The
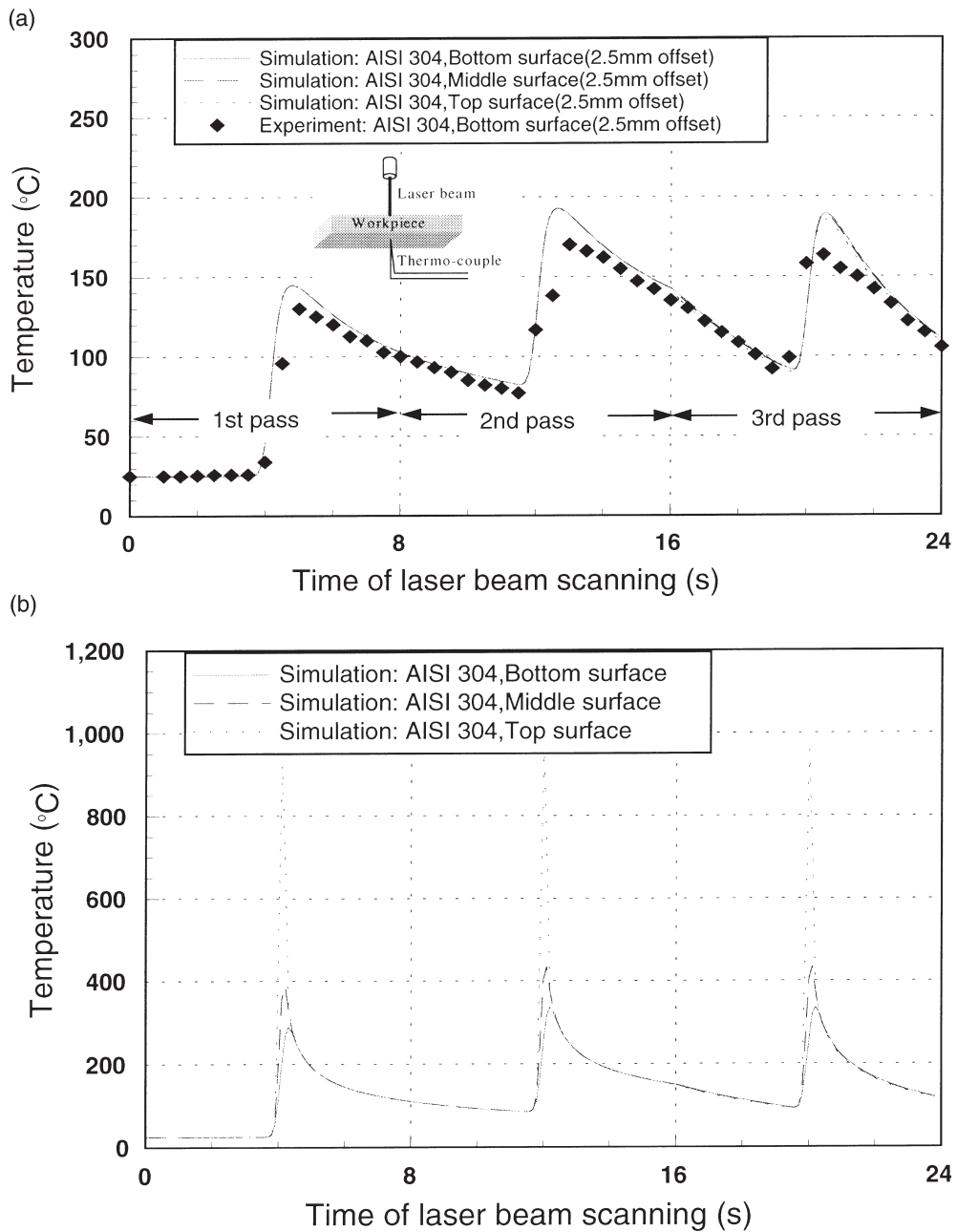
(a)



(b)



Fig. 6.  Temperature distribution with time of laser beam scanning (AISI 304, $P$=250 W, $v$=10 mm/s, $T$=1.5 mm). (a) Comparison of simulation results with experimental results; (b) Simulation results.
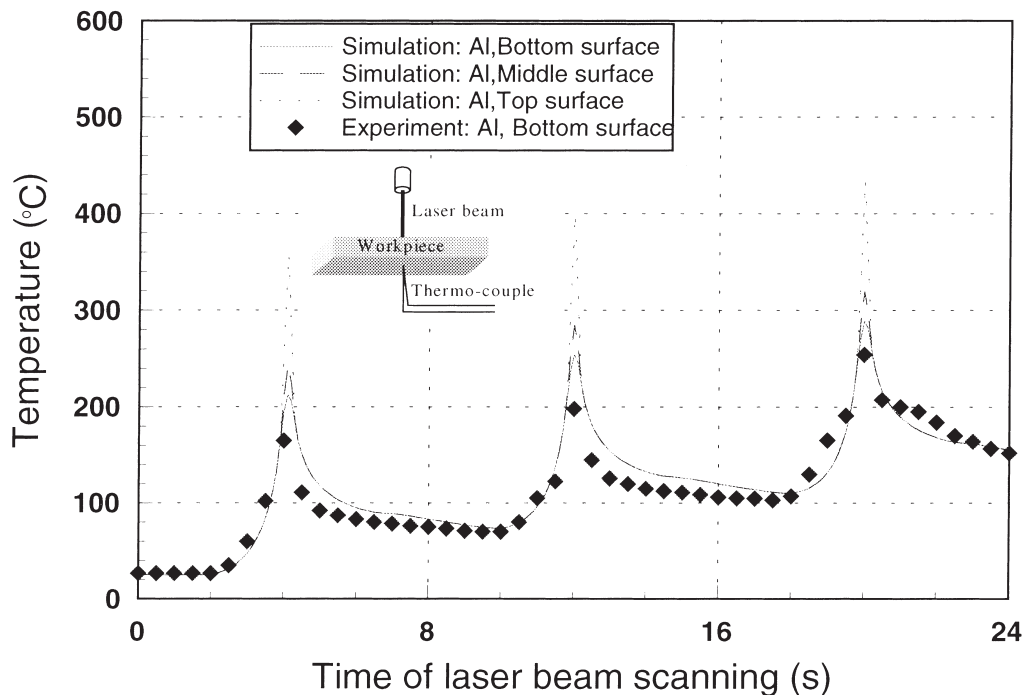
Fig. 7.   Temperature distribution with time of laser beam scanning (aluminum, $P$=500 W, $v$=10 mm/s, $T$=1.5 mm).

bending angle decreases with an increase in thickness in relation to the laser power and the scanning speed. Fig. 11 shows the relationship between the number of scanning passes and the bending angle for each different sheet metal thickness. The relatively thin sheet metal is more easily bent due to its less heat conduction resulting in higher peak temperature, higher temperature distribution and to more expansion at the top surface of the plate. Fig. 12 shows the relationship between the number of scanning passes and the bending angle for the different scanning speeds. For aluminum, for scanning speeds of 10 and 20 mm/s, the bending angles did not change; however, for higher scanning speed (40 mm/s) the bending angle is much smaller than in the case of lower scanning speeds. For stainless steel AISI 304, the bending angles are not so affected by the scanning speeds. Therefore there is an optimized process for scanning speed, or in other words, the larger bending angle could be obtained with better quality, faster speed, less time and less power. Fig. 13 shows the relationship between the number of scanning passes and bending angles for the different laser powers. For aluminum, the relationship between laser power and bending angle appears strongly nonlinear. Because when lower power, say $P$=250 W, is used, the temperature gradient along the thickness is not high enough to cause a large bending angle, so that the bending angle is very small. But when high power, say $P$=800 W, is used, the material on the top surface will be molten, so that the compressive stress is getting smaller, which results in the bending angle increasing nonlinearly. The larger bending angles could be achieved with a laser power of 500 W.

The microscopic photographs of the stainless steel AISI 304 after 4 line passes, with laser beams of 2 mm and 1 mm diameters (Fig. 14) illustrate that the area very close to the top
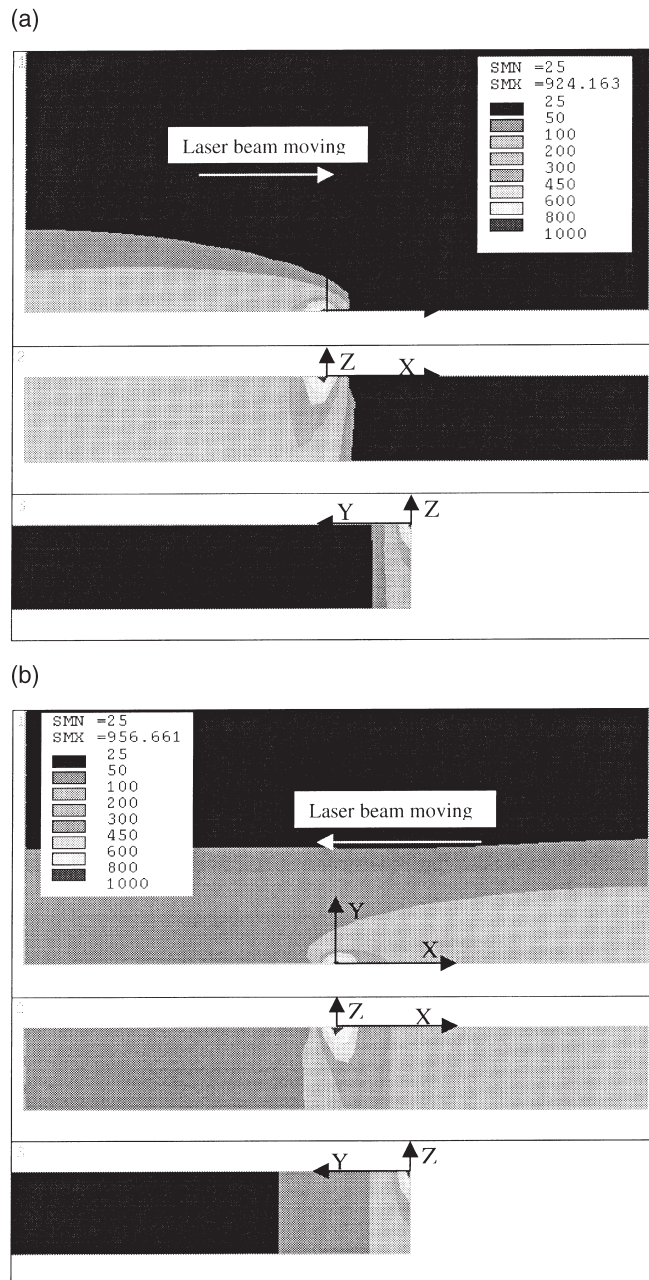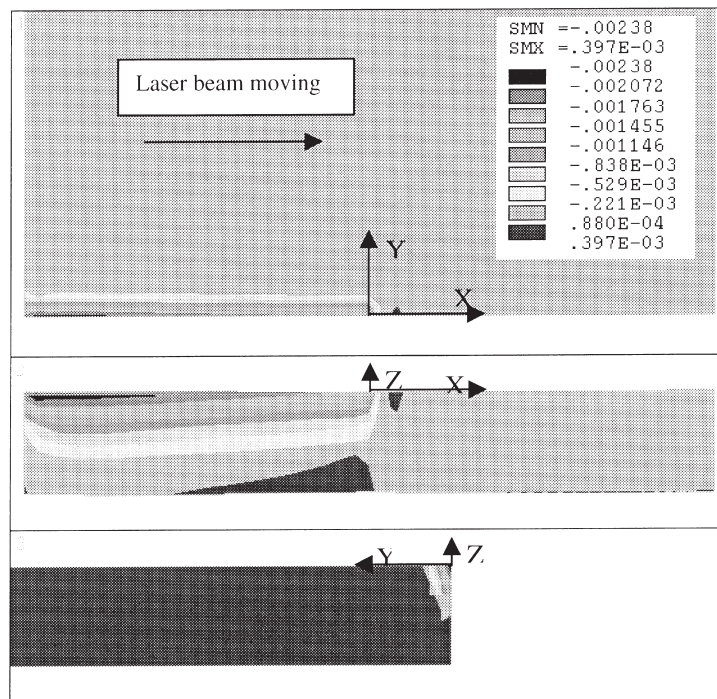
(a)



(b)



Fig. 8.   Temperature distribution during laser beam scanning by simulation (AISI 304, P=250 W, $v$=10 mm/s, $T$=1.5 mm). (a) Laser beam scanning on $x$=0 during 1st pass; (b) Laser beam scanning on $x$=0 during 2nd pass.
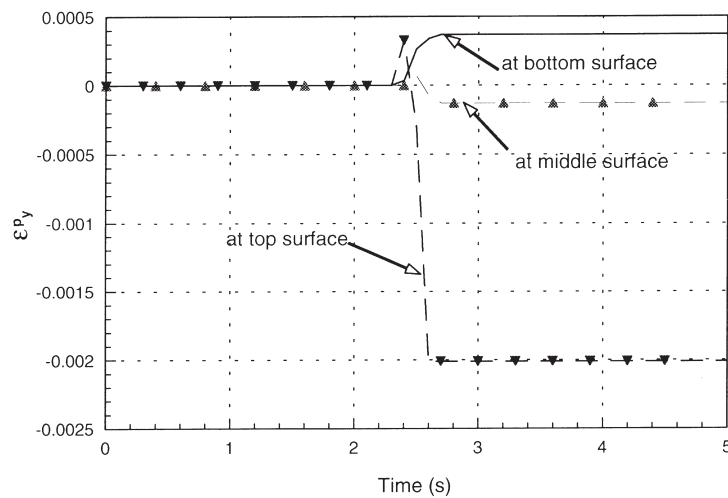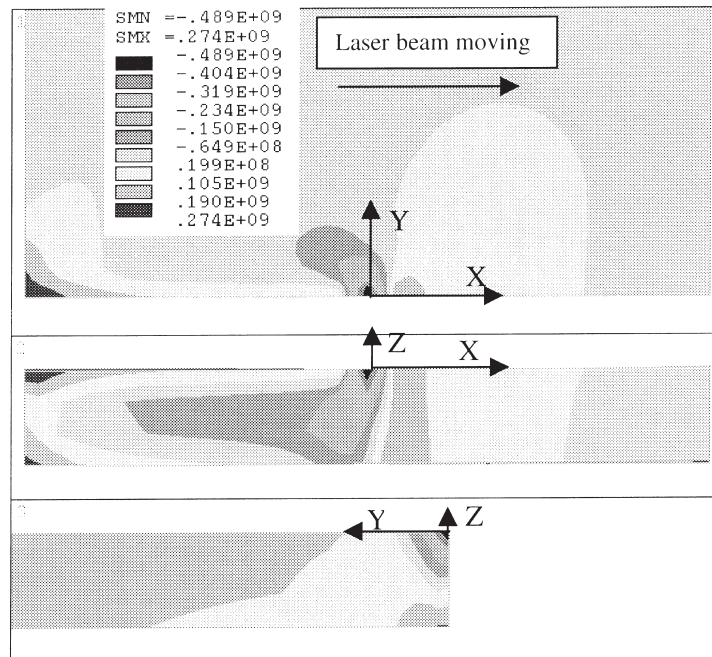
(a)



(b)



Fig. 9.   Distribution of plastic strain $\varepsilon_y^p$ during laser beam scanning of the 1st pass by simulation (AISI 304, $P$=250 W, $v$=10 mm/s, $T$=1.5 mm). (a) $\varepsilon_y^p$ on $x$=0; (b) $\varepsilon_y^p$ with time at different layers ($x$=0, $y$=0, $z$=0, 0.75 and 1.5 mm).
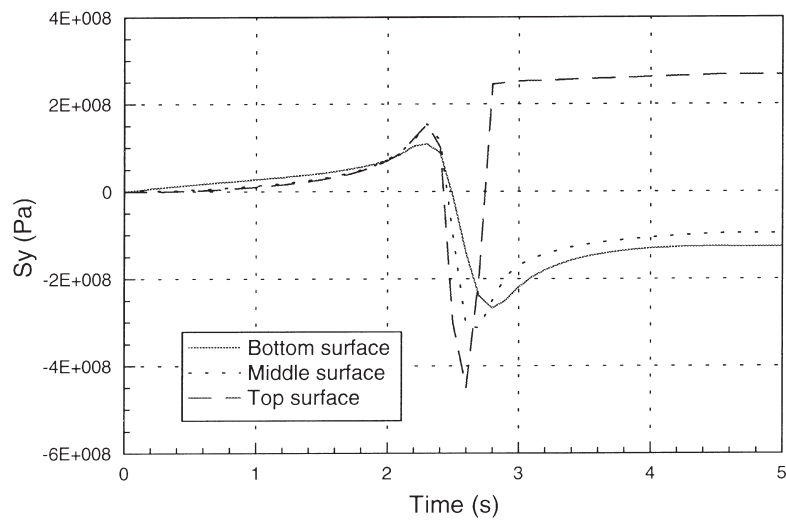
(a)



(b)



Fig. 10.   Distribution of stress $\sigma_y$ during laser beam scanning of the 1st pass by simulation (AISI 304, $P$=250 W, $v$=10 mm/s, $T$=1.5 mm). (a) $\sigma_y$ on $x$=0; (b) $\sigma_y$ with time at different layers ($x$=0, $y$=0, $z$=0, 0.75 and 1.5 mm).
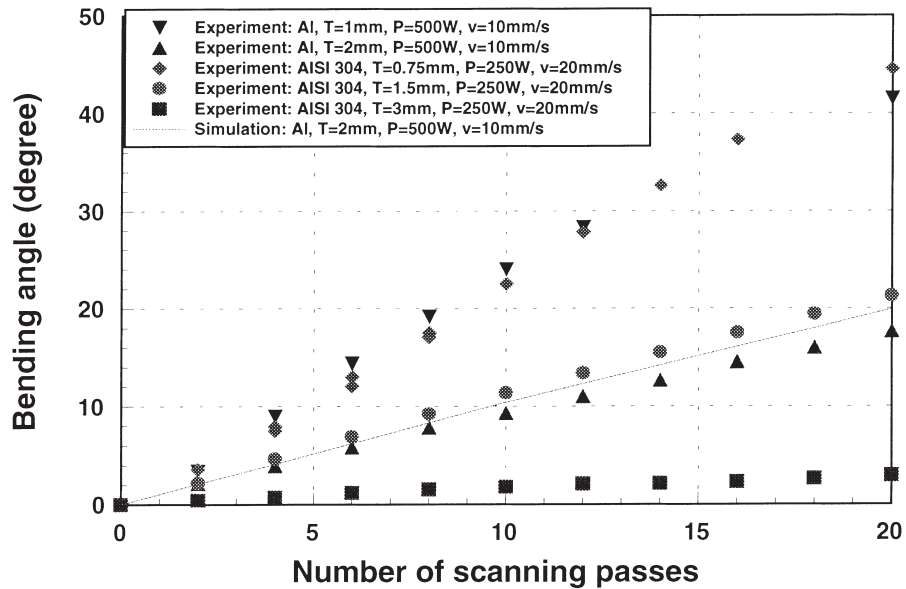
Fig. 11.   Relationship between scanning pass and bending angle with different thickness.
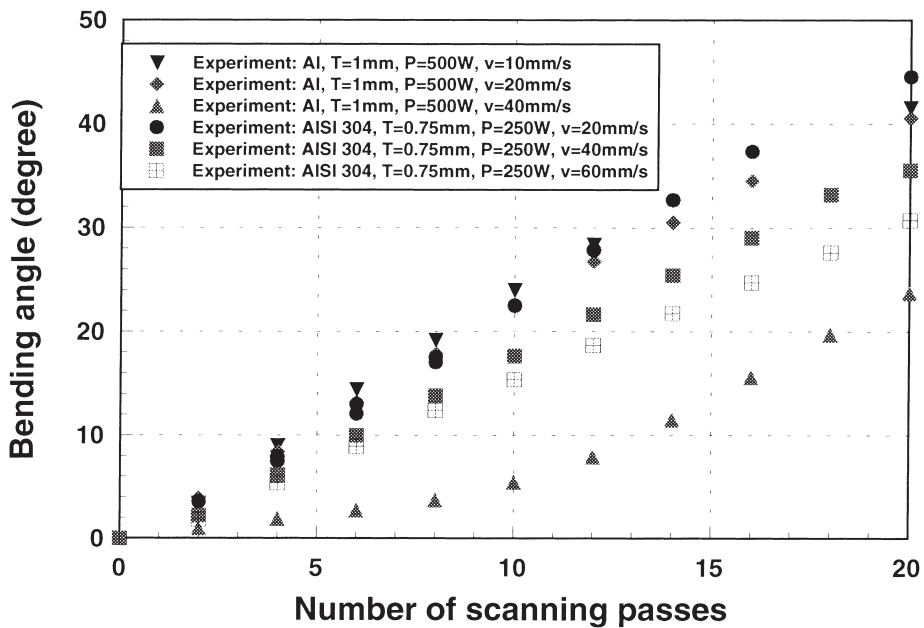
Fig. 12.   Relationship between scanning pass and bending angle with different scanning speed.
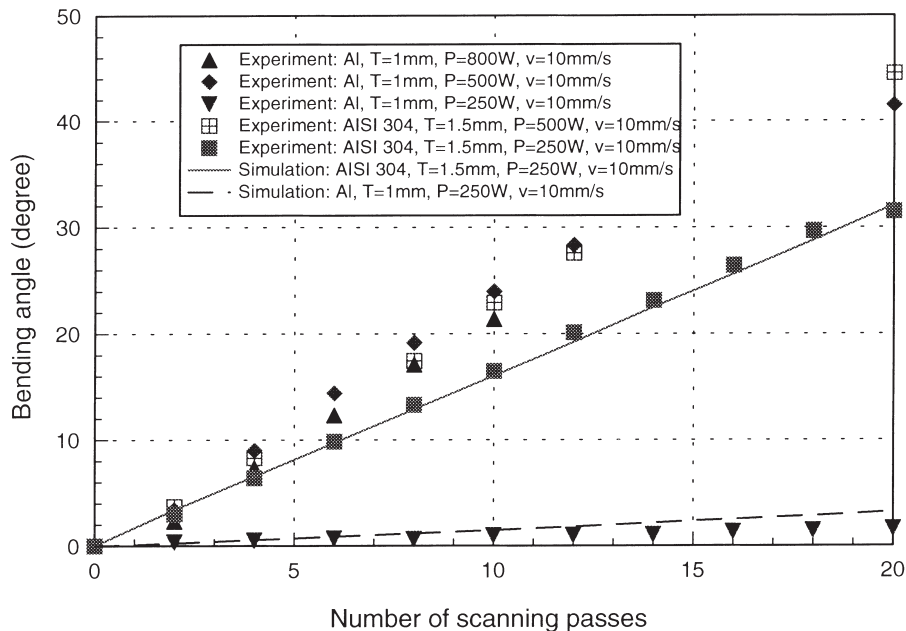
Fig. 13.   Relationship between scanning pass and bending angle with different laser power.

surface has been recrystallized after laser-forming. As mentioned earlier, the top surface undergoes significant plastic deformation at a temperature above the recrystallization temperature. Laser-forming may impart some beneficial properties to the workpiece. It can be seen that the microstructure is free of cracks, and harmful effects on the structure of the sheet metal in both cases, although the recrystallized grain sizes and the orientations of the grain are quite different from that before laser bending.

A Knoop micro-hardness trace was also performed across the welded microstructure on each sample to evaluate the change in material properties related to the various bending parameters. A load of 300 g and a dwell time of 15 s were used. A total of 13 measurements were taken, centering on the middle of the weld bead. The trace on each sample was at approximately the same depth of 0.0125 mm. However, the difference in the morphologies of the weld beads and the curvature of the plates hindered the consistency of the test locations. The results for both 2 mm and 3 mm plates are shown in Fig. 15. The approximate width of the resolidified region is also indicated in the figure, showing agreement with the metallographic measurements given above. In the area melted by the laser beam, for the plate with the 2 mm thickness in the central line of the weld bead, the hardness is 195.9 and 222.7 kN after 4 and 8 passes, respectively. Around this position, after 8 passes, the hardness is approximately constant. This result can be seen in Fig. 15(a) where the hardness values are plotted and a horizontal line is obtained in the width area of the resolidified region. Outside of the area, the values increase by 25% and drop to the value of the centerline when the position relative to centerline goes to 2.5 mm. It can be seen in Fig. 15(b) that on the 3 mm plate no significant variation is obtained in the approximate width of the weld. It can be said that in the melt area, the hardness is constant and independent of the number of laser beam passes. The same is true of the 2 mm plate: in the neighbourhood of the
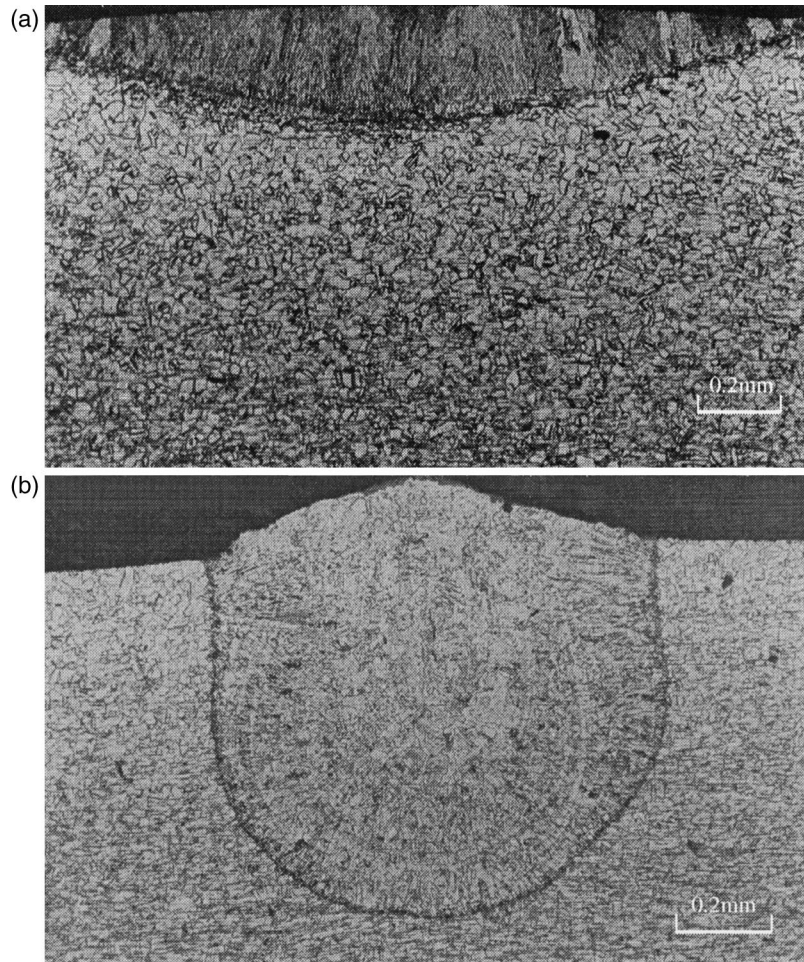
Fig. 14.   Microscopic photographs of AISI 304 sheet metal after 4 line passes: (a) 2 mm thick with 2 mm diameter laser beam; (b) 3 mm thick with 1 mm diameter laser beam.

resolidified area, where the metal was affected by heat but was not melted, the hardness increased by 25% and decreased at 2.5 mm away form the centerline to a value comparable to the hardness in the centerline of the melted area.

## 7. Conclusions

A 3-D computer simulation and an on-line experimental investigation of sheet metal bending using laser beam scanning have been performed. The following conclusions have been reached.

1. A 3-D FEM simulation system has been developed which includes a nonlinear transient indirect
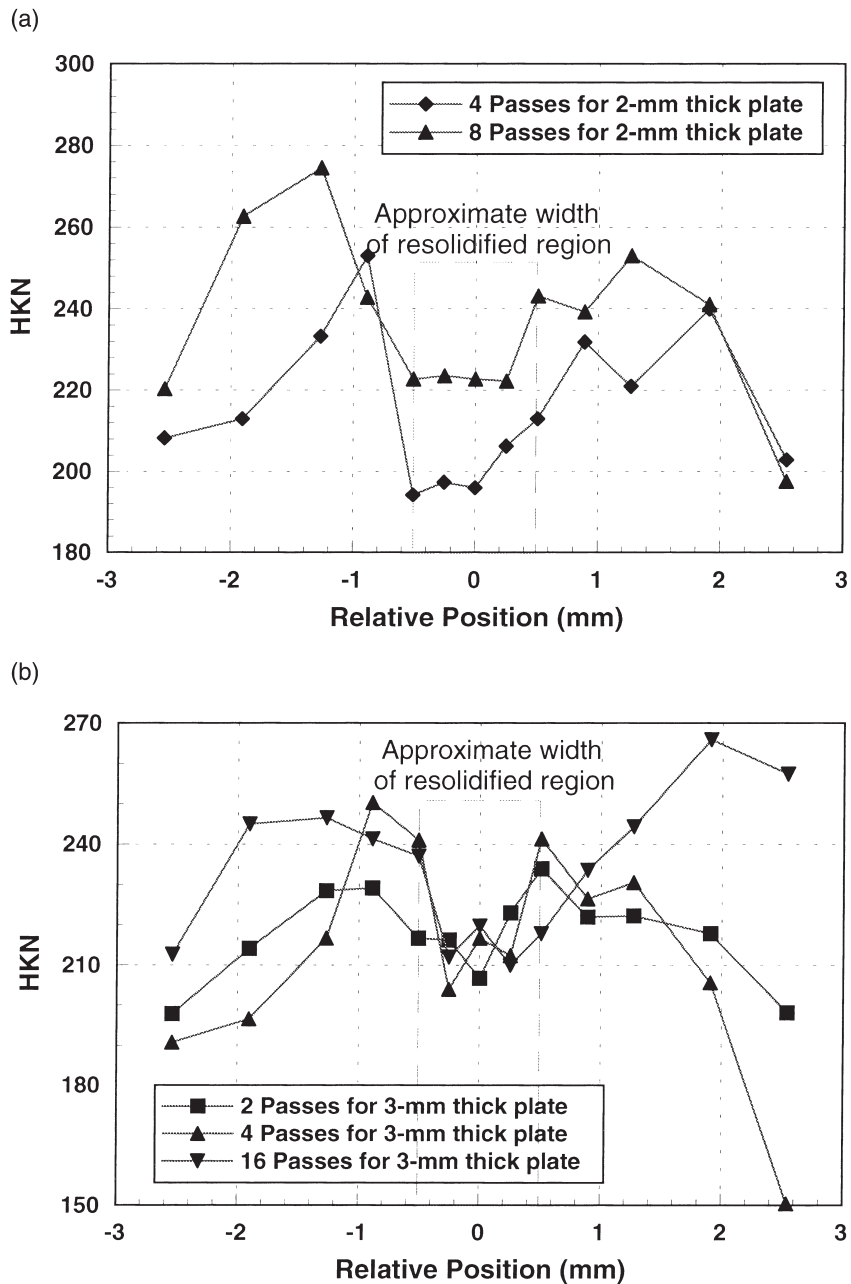
(a)



(b)



Fig. 15.   Knoop microhardness results for AISI 304 sheet metal after laser beam scanning; (a) for 2 mm plates; (b) for 3 mm plates.

coupled thermal-structural analysis accounting for the temperature dependency of the thermal and mechanical properties of the materials. The bending angle, distribution of stress–strain, temperature and residual stress can be obtained by computer simulation. The bending action is caused by the thermal stress in the sheet upon the plastic deformation due to the extremely-rapid heating and cooling process during the laser irradiation. The bending is in the direction away from the laser beam during heating and toward the laser beam during cooling. The available simulated temperature distributions and bending angles are in agreement with the experimental results.

2. The bending angle is affected by the mechanical and thermal properties of the sheet metal material, and the process parameters. It is increased with the number of laser beam scanning passes, decreased with the thickness of the sheets and is a function of the laser power and the laser beam scanning speed in the given experimental conditions. The optimized sheet metal bending process using laser beam scanning could be performed.

3. Laser beam scanning can bend sheet metal with quality results. It has no harmful effects on microstructure of the plate, and does not produce any cracks or porosity in the stainless steel plate.

## Acknowledgements

## References

[1] J. Magee, K.G. Watkins, W.M. Steen, Advances in laser forming, Journal of Laser Application 10 (1998) 235–246.

[2] H. Frackiewicz, High-technology metal forming, Industrial Laser Review, October (1996) 15–17.

[3] M. Gremaud, J.D. Wagniere, A. Zryd, W. Kurz, Laser metal forming: process fundamentals, Surface Engineering 12 (3) (1996) 251–259.

[4] K. Masubuchi, H. Shimizu, A review of past and current studies related to metal forming by laser line heating, submitted from M.I.T. to Rocketdyne, October 1995.

[5] H. Arnet, F. Vollertsen, Extending laser bending for the generation of convex shapes, ImechE Part B, Journal of Engineering Manufacture 209 (1995) 433–442.

[6] M. Pridham, G. Thomson, Laser forming: a force for the future? Materials World, Journal of the Institute of Materials 2 (11) (1994) 574–575.

[7] M. Geiger, Synergy of laser material processing and metal forming, Annals of the CIRP 43 (1994) 563–570.

[8] R.W. McCarthby, Thermomechanical forming of steel plates using laser line heat, PhD thesis, Massachusetts Institute of Technology, 1985.

[9] K. Masubuchi, Studies at M.I.T. related to applications of laser technologics to metal fabrication, Proceedings of LAMP, 1992.

[10] Y. Namba, Laser forming of metals and alloys, Proceedings of LAMP, 1987.

[11] Y. Namba, Laser forming in space, in: C.P. Wang (Ed.), Proceedings of the International Conference on Lasers '85, Osaka, Japan, 1986, pp. 403–407.

[12] K. Scully, Laser line heating, Journal of Ship Production 3 (4) (1987) 237–246.

[13] A.K. Kyrsanidi, T.B. Kermanidis, S.G. Pantelakis, Numerical and experimental investigation of the laser forming process, J. Mater. Processing Technology 87 (1999) 281–290.

[14] Z. Ji, S. Wu, FEM simulation of the temperature field during the laser forming of sheet metal, J. Mater. Processing Technology 74 (1998) 89–95.

[15] W. Li, M. Geiger, F. Vollertsen, Study on laser bending of metal sheets, Chinese Journal of Lasers 25 (9) (1998) 859–864.

[16] G. Chen, X. Xu, C.C. Poon, A.C. Tam, Experimental and 2-D numerical studies on micro-scale bending of stainless steel with pulsed laser, in: Proceedings of the ASME Heat Transfer Division, HTD-vol. 361-4, 1998, pp. 49–56.

[17] Y.-C. Hsiao, Finite element analysis of laser forming, PhD thesis, Massachusetts Institute of Technology, 1997.

[18] N. Alberti, L. Fratini, F. Micari, M. Cantello, G. Savant, Computer aided engineering of a laser assisted bending process, Laser Assisted Net shape Engineering 2, in: Proceedings of the LANE'97, vol. 2, 1997, pp. 375–382.

[19] Y.-C. Hsiao, H. Shimizu, L. Firth, W. Maher, K. Masubuchi, Finite element modeling of laser forming, in: Proc. ICALEO'97, Section A, 1997, pp. 31–40.

[20] T. Nakagawa, A. Makinouchi, J. Wei, T. Shimizu, Application of laser stereolithography in FE sheet-metal forming simulation, J. Mater. Processing Technology 50 (1995) 318–323.

[21] F. Vollersten, S. Holzer, 3D-thermomechanical simulation of laser forming, Simulation of Material Processing, 1995.

[22] K.U. Odumodu, Finite element simulation of laser shaping, PhD Thesis, University of Detroit-Mercy, 1995.

[23] N. Alberti, L. Fratini, F. Micari, Numerical simulation of the laser bending process by a coupled thermal mechanical analysis, in: Laser Assisted Net Shape Engineering, Proceedings of the LANE'94, vol. 1, 1994, pp. 327–336.

[24] F. Vollertsen, An analytical model for laser bending, Laser in Engineering 2 (1994b) 261–276.

[25] F. Vollertsen, M. Geiger, W.M. Li, FDM- and FEM-simulation of laser forming: a comparative study, in: Advanced Technology of Plasticity 1993–Proceeding of the Fourth International Conference on Technology of Plasticity, 1993, pp. 1793–1798.

[26] ANSYS Theory Manual, Release 5.3, ANSYS Inc., USA, June 1996.

[27] P.D. Harvey (Ed.), Engineering Properties of Steel American Society for Metals, Metals Park, OHIO 44073, 1982.

[28] E.A. Brandes, G.B. Brook (Eds.), Smithells Metals Reference Book seventh ed., Reed Educational and Professional Publishing Ltd, 1998.

[29] R. Kovacevic, R. Mohan, H. Beardsley, Monitoring of thermal energy distribution in abrasive waterjet cutting using infrared thermography, ASME J. Manuf. Sci. and Engng. 118 (1996) 555–563.